Electronic Supplementary Material (ESI) for Journal of Materials Chemistry A

Supplementary information for

Emulsion-templated bicontinuous carbon network electrodes for use in 3D microstructured batteries

Habtom Desta Asfaw, Matthew Roberts, Reza Younesi and Kristina Edström*

Department of Chemistry-Ångström Laboratory, Uppsala University, Box 538, SE-75121 Uppsala, Sweden

Table S1. Summary of the performance obtained for 3D electrodes reported in the literature.

		Slow Rate Capacity/ µA h cm^{-2}		*High Rate Capacity/ µA h cm^{-2}*	
Material	**Ref**	**Rate**	**Capacity**	**Rate**	**Capacity**
Spin-dried $LiFePO_4$/RVC (4 coats)	Roberts et al. [1]	~C/4	~1500	~17C	~849
Electrodeposited MnO_2/RVC	Johns et al. [2]	~C/20	~3000	2C	~150
Electrodeposited CuS/ silicon microchannels	Mazor et al. [3]	~C/8	~1100	~2C	~500
Electrophoretically deposited $LiFePO_4$/ silicon micro channels	Mazor et al. [4]	~C/50	~2300	N/A	N/A
Spray Coated $LiCoO_2$/ Aluminum pillars	Shaijumon et al. [5]	~C/10	~125	~7C	~85
TiO_2 Nanotubes	Wei et al. [6]	C/10	~600	5C	300
Cu_2Sb	Perre et al. [7]	C/10	~280	5C	~150

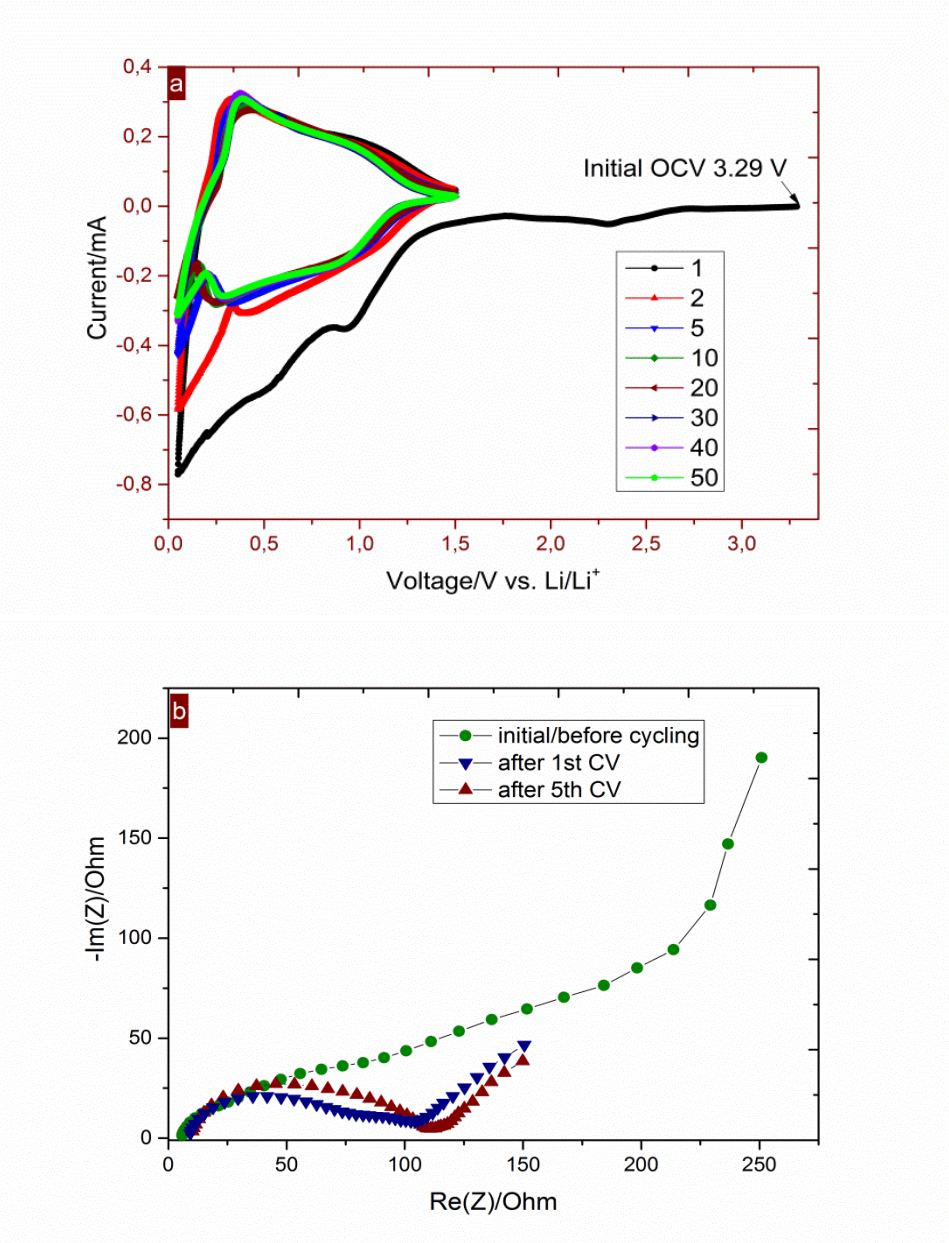

Figure S1: Cyclic voltammograms (a) and Impedance plots (b) of polyHIPE-derived carbon foams. The first impedance measurement is made at the initial OCV 3.29 V versus Li and typifies double layer charging at porous electrodes.[8] The subsequent plots correspond to measurements conducted on the carbon foam cycled between 0.05 and 1.5 V versus Li and show that different interfacial phenomena are involved: SEI formation and lithium insertion/de-insertion.[9]

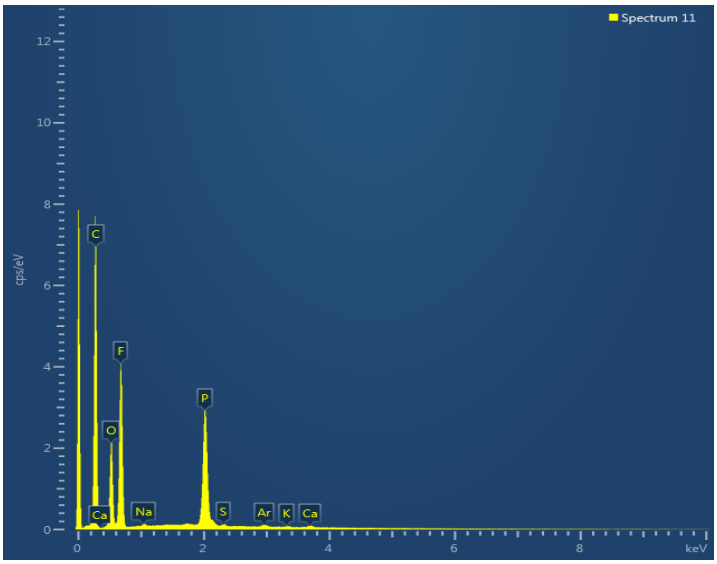

Fig. S2: EDX spectrum of cycled carbon foam shown in Figure 6.

XPS Study SEI layer

To study the pristine and the carbon foams after 55 cycles further we used XPS measurements to more accurately determine the surface composition. A summary of the data collected from the XPS measurement is given in Figures S3 and S4. Figure S3(a) shows the relative elemental composition on the surface of these samples assuming a uniform distribution of elements. The surface of the pristine electrode is mainly composed of C as expected. However, small amounts (~1.5%) of F, S, and Ca were observed on the surface of the pristine electrode. These three elements are impurities introduced during the polymerization and sulfonation steps undertaken during the foam preparation. We can see that after the foam is cycled as an anode the surface composition is mainly composed of F and Li. These elements originate from the decomposition of the electrolyte and formation of the SEI layer similar to previously reported results regarding formation of SEI on graphite [10].

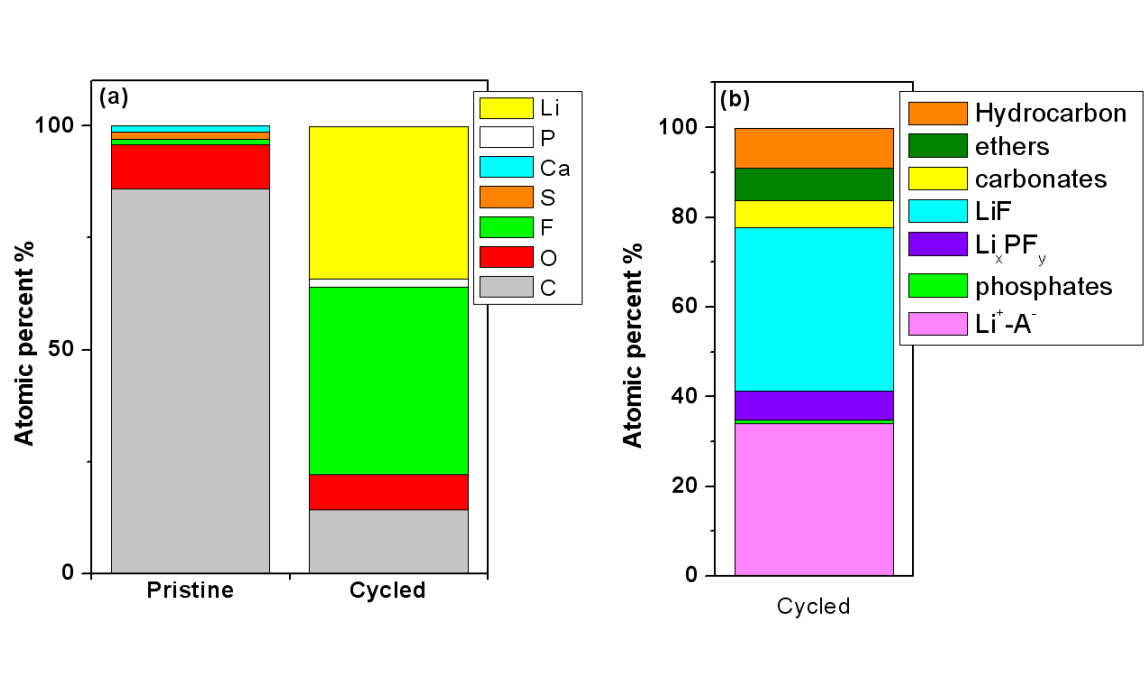

Fig. S3: (a) The relative element surface compositions of pristine and cycled electrodes. (b) The relative molecular composition of the surface of the cycled electrode (Li^+-A^- represents all other unidentified lithium containing compounds).

The high-resolution spectra of the observed elements are presented in Figure S4. For the pristine electrodes significant peaks were only observed in the C 1s and O1s spectra. The C 1s spectrum of the pristine electrode appears similar to a typical spectra of graphite in which the graphite and hydrocarbon peaks appear dominant at binding energies of 284.4 and 285 eV, respectively [11]. The XPS spectra for the cycled electrode are much more complicated with significant contributions from F, O, C, P and Li. The F 1s and P 2p spectra of the cycled

electrodes imply that $LiPF_6$ salt has decomposed and formed species contained within the passive surface layer. The F 1s spectrum consists of two peaks at the binding energies of 685.1 and 687.4 eV representing LiF and $Li_xPF_y/Li_xPO_yF_Z$, respectively. The P 2p spectrum confirms the decomposition of the $LiPF_6$ salt into two chemical environments at 134.7 and 137.5 eV respectively each with a double spin-orbit split (for the two chemical states of phosphorous, P $2p_{3/2}$ and P $2p_{1/2}$) . The former peak originates from P-O bond containing compounds (e.g. phosphates) while the latter peak represents Li_xPF_y. The C 1s spectrum shows that the SEI layer contains carbonate and ether groups which are typically attributed to products from electrolyte breakdown which occur during SEI formation. The species present in the SEI layer are summarized in Figure S3(b). The XPS spectra indicate that the SEI is composed of decomposition products formed of the salt and the solvent during cycling which is similar to that observed on the SEI of graphite electrodes [12-14].

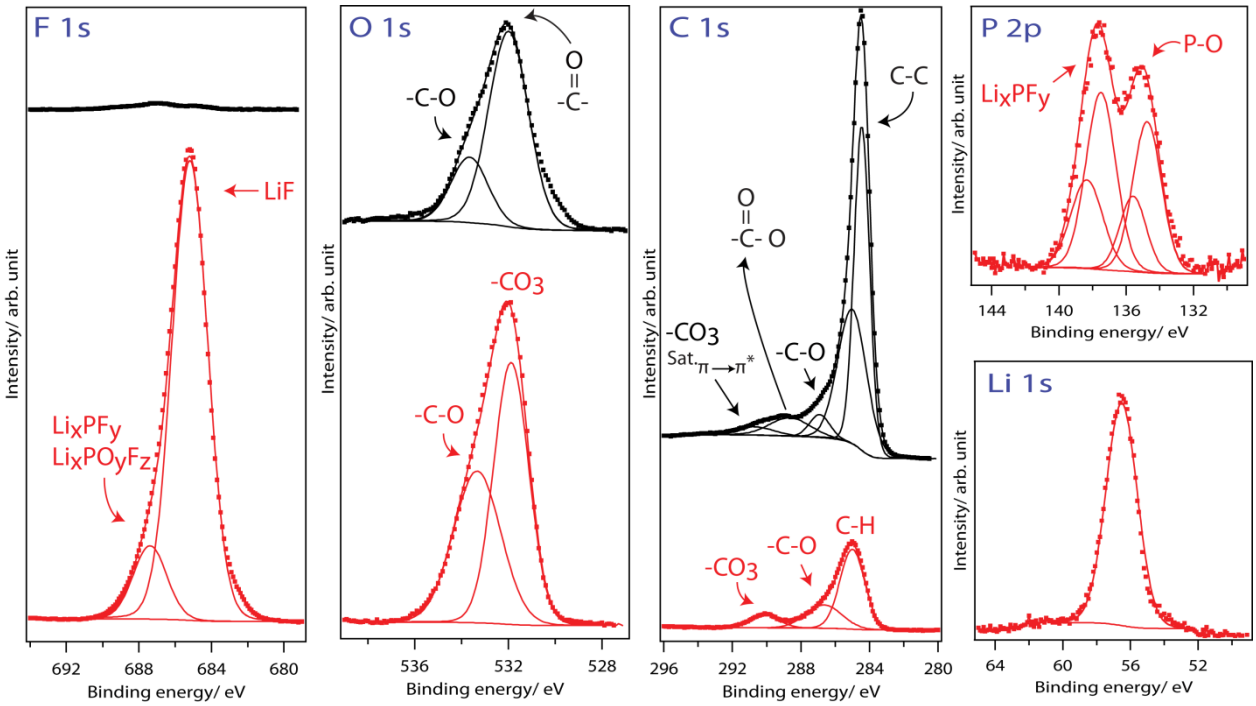

Fig. S4: XPS measurements of pristine and cycled polyHIPE-derived carbon foam synthesized at 700°C.

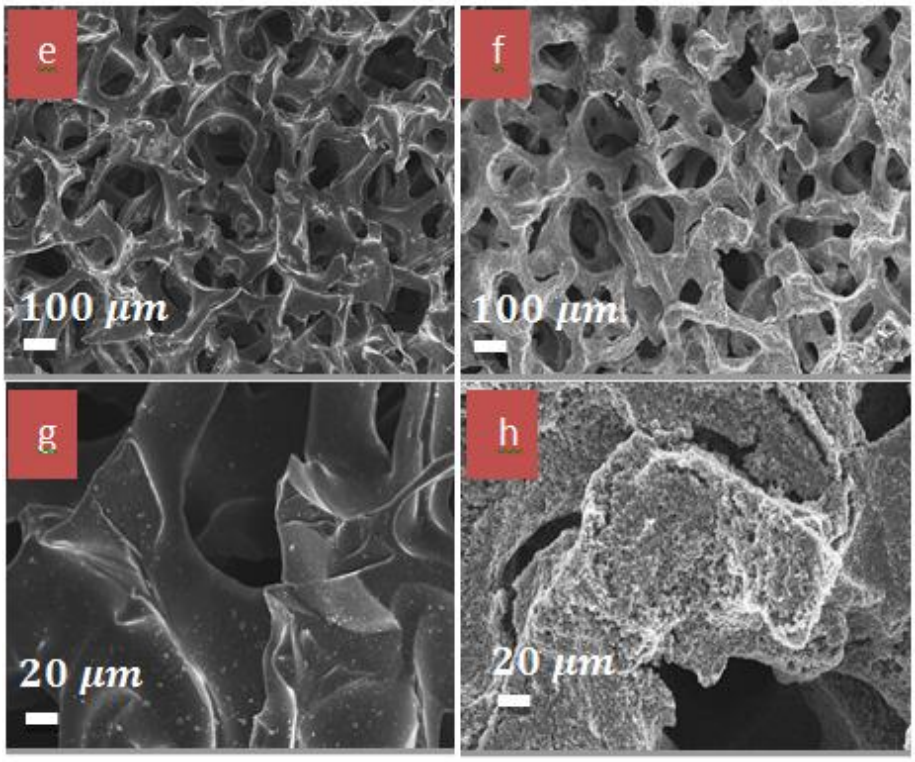

Fig. S5: Scanning electron micrographs of bare and PANI-coated RVC carbon (bare: e and g, coated: f and h) foams taken at two different magnifications. 10 cycles of deposition were performed using cyclic voltammetry. Note: Each micrograph in the second row represents same image as the one directly above it but is taken at a higher magnification.

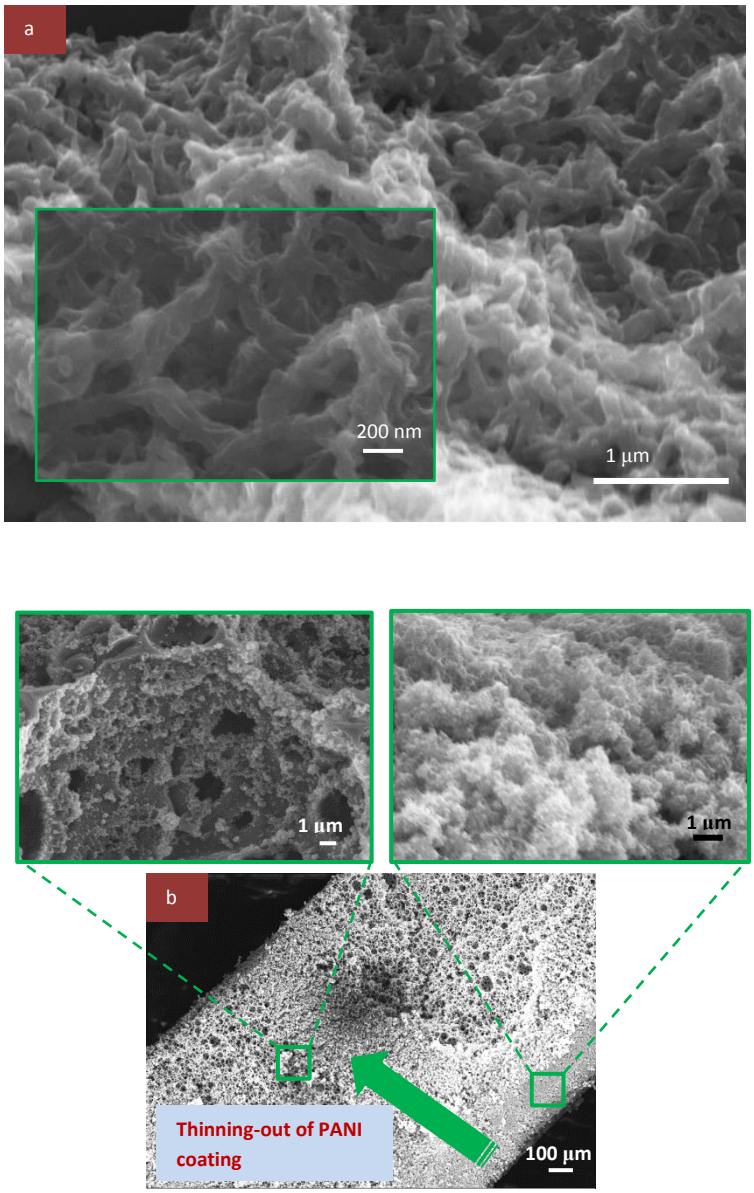

Fig. S6 : SEM images of PANI coating on polyHIPE-derived carbon foams (a) It can be noted that the PANI layer is very porous with more or less consistent coating. Inset image shows randomly oriented PANI nanofibers. (b) The amount of PANI tapers off as one goes from the edges to the centre of the carbon foam as indicated in the high-magnification SEMs.

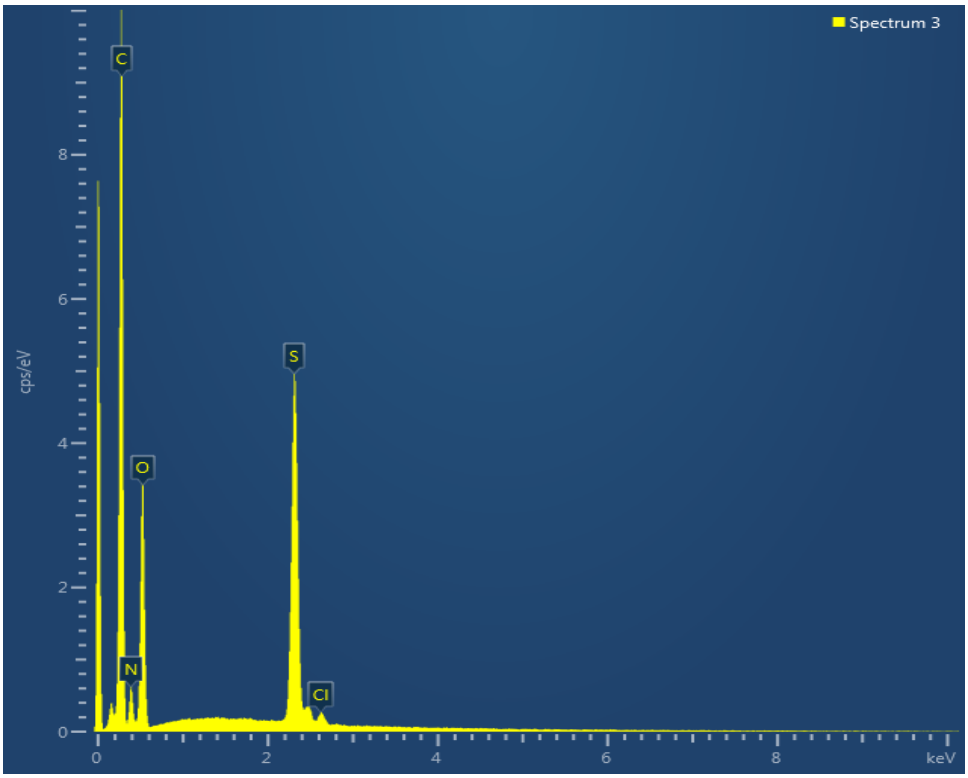

Fig. S7: EDX spectrum of polyaniline layer deposited electrochemically on polyHIPE carbon.

Extending the Potential Window of Polyaniline

In Figure S6, the electrochemical cycling window of the PANI film is increased to 2.5 to 4.0 V vs. Li/Li^+. This enhances the capacity per footprint area by approximately 50 µA h cm^{-2}. The reaction can be seen to proceed with a high coulombic efficiency reaching in excess of 99% and a hysteresis of 0.15 V. It is also noted that no significant parasitic or corrosion reactions are seen during the discharge indicating that the carbon is an inert substrate.

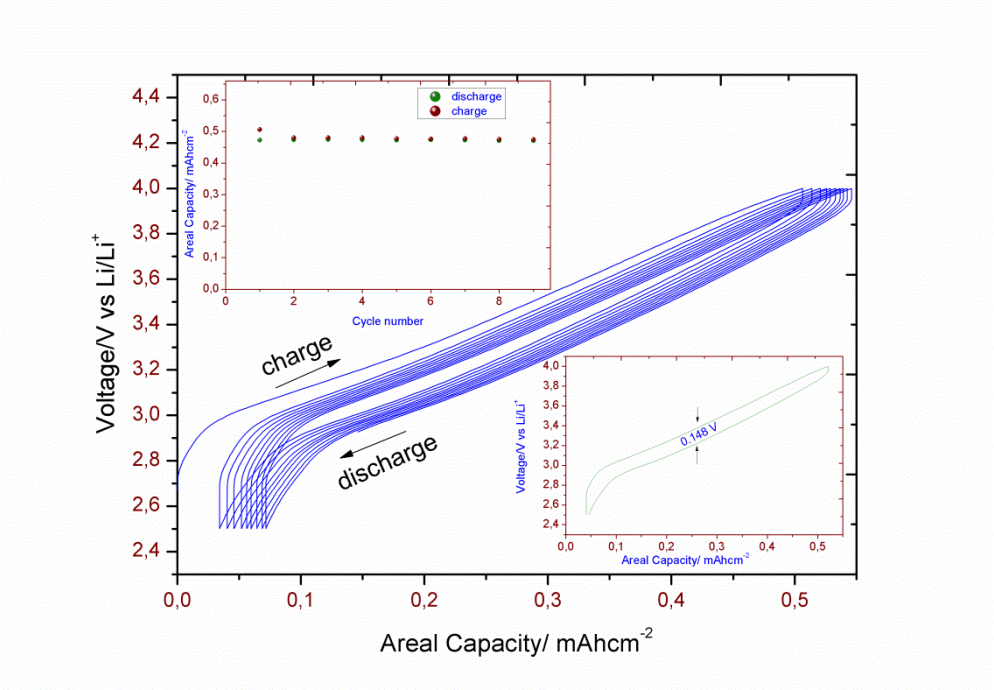

Fig. S8: Cycling performance of PANI on polyHIPE-derived carbon foam substrate vs. lithium at about 0.13 $mAcm^{-2}$ is shown. Insets: top-areal charge and discharge capacities as a function of cycle number. A coulombic efficiency exceeding 99% is observed. Bottom-voltage profile for the second cycle with an indication of hysteresis between charge and discharge.

References

1. M. Roberts, A. F. Huang, P. Johns and J. Owen, *J. Power Sources*, 2013, **224**, 250-259.
2. P. Johns, M. Roberts and J. Owen, *J. Mater. Chem.*, 2011, **21**, 10153-10159.
3. H. Mazor, D. Golodnitsky, L. Burstein and E. Peled, *Electrochem. Solid-State Lett.*, 2009, **12**, A232-A235.
4. H. Mazor, D. Golodnitsky, L. Burstein, A. Gladkich and E. Peled, *J. Power Sources*, 2012, **198**, 264-272.
5. M. M. Shaijumon, E. Perre, B. Daffos, P.-L. Taberna, J.-M. Tarascon and P. Simon, *Adv. Mater.*, 2010, **22**, 4978-4981.

6. W. Wei, G. Oltean, C.-W. Tai, K. Edstrom, F. Bjorefors and L. Nyholm, *Journal of Materials Chemistry A*, 2013, **1**, 8160-8169.
7. E. Perre, P. L. Taberna, D. Mazouzi, P. Poizot, T. Gustafsson, K. Edström and P. Simon, *J. Mater. Res.*, 2010, **25**, 1485-1491.
8. L. Permann, M. Lätt, J. Leis and M. Arulepp, *Electrochim. Acta*, 2006, **51**, 1274-1281.
9. B. V. Ratnakumar, M. C. Smart and S. Surampudia, in *Battery Conference on Applications and Advances, 2002. The Seventeenth Annual*, 2002, pp. 273-277.
10. M. Herstedt, D. P. Abraham, J. B. Kerr and K. Edström, *Electrochim. Acta*, 2004, **49**, 5097-5110.
11. R. I. R. Blyth, H. Buqa, F. P. Netzer, M. G. Ramsey, J. O. Besenhard, P. Golob and M. Winter, *Appl. Surf. Sci.*, 2000, **167**, 99-106.
12. A. M. Andersson and K. Edström, *J. Electrochem. Soc.*, 2001, **148**, A1100.
13. A. M. Andersson, A. Henningson, H. Siegbahn, U. Jansson and K. Edström, *J. Power Sources*, 2003, **119-121**, 522-527.
14. S. Leroy, F. Blanchard, R. Dedryvère, H. Martinez, B. Carré, D. Lemordant and D. Gonbeau, *Surf. Interface Anal.*, 2005, **37**, 773-781.